Science

AAAS

This copy is for your personal, non-commercial use only.

though at low oxygen, placental hemoglobin binding affinity for O_2 is modified by pH (i.e., the Bohr effect), with exceptions, few extant mammals reproduce above elevations of ~4500 m, corresponding to atmospheric oxygen levels in the Early Jurassic ([15]).

Whereas a bolide impact at the Cretaceous-Tertiary (K-T) boundary and the ensuing extinction of dinosaurs provided ecological opportunity for the radiation of placental mammals, the rise of oxygen in the Eocene corresponds to a large increase in average mammalian body size ([27]). The density of capillaries per unit muscle scales to the 0.87 power of size in mammals ([28]); hence, larger animals require high ambient O_2 levels to obtain maximal metabolic rates. Comprehensive study of body mass of nearly 2000 fossil mammals in the North American record indicates a steady expansion in size range throughout the Cenozoic, tracked by mean body size due to the static lower limit of size ([27]). Data show a rapid increase from small to medium-sized mammals in the first few million years after the K-T event (Fig. 2). This size contrast is blurred slightly with the recent discovery of larger Cretaceous mammals ([29]), but this trend does not appear to be driven by oxygen. A second upward surge in mean body mass is recorded for the early through middle Eocene (50 to 40 Ma) ([27]), followed by further but less dramatic size increases through the Miocene. This trend tracks a change in oxygen. The early to middle Eocene, an interval characterized by the highest global mean annual temperatures and the broadest latitudinal span of warm subtropical to temperate faunas and floras for the Cenozoic, was also a time of high morphological disparity in North American placental mammals. One might infer that this indicates a proliferation of ecological roles in the North American mammalian fauna. Notably, many of the living placental orders appear in the early Eocene, and artiodactyls, the dominant large terrestrial herbivores today, underwent a massive radiation in the mid-Eocene ([27]). Data from other continents are more limited, but there is reason to argue that North America serves as a model for broader patterns, at least in the northern hemisphere. The substantially improving records in Europe and Asia, especially, will provide an interesting test of the pattern.

The data presented here provide evidence of a secular increase in atmospheric oxygen over the past 205 My that broadly corresponds with three main aspects of vertebrate evolution, namely endothermy, placentation, and size. Particularly notable are high stable O_2 levels during the time of placental mammal origins and diversification and a close correspondence between marked increases in both atmospheric oxygen levels and mammalian body size during the early to middle Eocene. Although increases in mammalian body size,

morphological disparity, and inferred ecological heterogeneity during this interval may have been influenced as well by other environmental factors such as warm global temperatures and the spread of tropical and subtropical habitats, the correlation between evolutionary changes in mammalian body size and increased atmospheric O_2 has a physiological basis related to placental mammal reproduction. The changes in oxygen appear to have been driven by tectonics and increased burial efficiency of organic matter on continental margins.

References and Notes

1. H. Tappan, in *Molecular Oxygen in Biology: Topics in Molecular Oxygen Research*, O. Hayaishi, Ed. (North-Holland, Amsterdam, 1974), chap. 3, pp. 81–135.
2. P. W. Hochachka, G. Somero, *Biochemical Adaptation: Mechanism and Process in Physiological Evolution* (Oxford Univ. Press, New York, 2002).
3. R. Garrels, A. Lerman, *Am. J. Sci.* **303**, 94 (1984).
4. H. D. Holland, *The Chemical Evolution of the Atmosphere and Oceans* (Princeton Univ. Press, Princeton, NJ, 1984).
5. R. A. Berner *et al.*, *Science* **287**, 1630 (2000).
6. R. A. Berner, D. E. Canfield, *Am. J. Sci.* **289**, 333 (1989).
7. L. Kump, M. Arthur, *Chem. Geol.* **161**, 181 (1999).
8. J. M. Hayes, H. Strauss, A. J. Kaufman, *Chem. Geol.* **161**, 103 (1999).
9. N. J. Shackleton, M. A. Hall, in *Initial Reports of the Deep Sea Drilling Project*, T. C. Moore Jr. *et al.*, Eds. (U.S. Government Printing Office, Washington, DC, 1984), vol. 74, pp. 613–619.
10. M. E. Katz *et al.*, *Mar. Geol.* **217**, 323 (2005).
11. R. A. Berner, *Geochim. Cosmochim. Acta* **65**, 685 (2001).
12. J. R. Reinfelder, A. M. L. Kraepeil, F. M. M. Morel, *Nature* **407**, 996 (2000).
13. R. F. Sage, in *Plant Biology*, R. F. Sage, R. K. Monson, Eds. (Academic Press, San Diego, 1999), pp. 3–16.
14. T. E. Cerling *et al.*, *Nature* **389**, 153 (1997).
15. R. B. Huey, P. D. Ward, *Science* **308**, 398 (2005).
16. P. G. Falkowski *et al.*, *Science* **305**, 354 (2004).
17. K. O. Emery, E. Uchupi, *Am. Assoc. Pet. Geol. Memoir* **17**, 532 (1972).
18. V. Smetacek, *Protist* **150**, 25 (1999).
19. R. L. Carroll, *Vertebrate Paleontology and Evolution* (Freeman, New York, 1988).
20. R. J. Asher *et al.*, *Science* **307**, 1091 (2005).
21. P. Else, A. Hulbert, *Am. J. Physiol. Regul. Integr. Comp. Physiol.* **240**, R3 (1981).
22. W. J. Murphy *et al.*, *Science* **294**, 2348 (2001).
23. M. S. Springer, M. J. Stanhope, O. Madsen, W. de Jong, *Trends Ecol. Evol.* **19**, 430 (2004).
24. R. Shine, *Annu. Rev. Ecol. Evol. Syst.* **36**, 10.1146/annurev.ecolsys.36.102003.152631 (2005).
25. J. Mortola, *Respiratory Physiology of Newborn Mammals: A Comparative Perspective* (Johns Hopkins Univ. Press, Baltimore, 2001).
26. R. Andrews, *Physiol. Biochem. Zool.* **75**, 145 (2002).
27. J. Alroy, *Syst. Biol.* **48**, 107 (1999).
28. E. Weibel, H. Hoppeler, *J. Exp. Biol.* **208**, 1635 (2005).
29. Y. Hu, J. Meng, Y. Wang, C. Li, *Nature* **433**, 149 (2005).
30. M. Ghil *et al.*, *Reviews of Geophysics* **40**, 10.1029/2000RG000092 (2002).
31. Based on fossil appearance dates and ghost lineage analysis, the split between the crown group Placentalia and its nearest eutherian sister taxon is about 80 Ma, but no member of crown Placentalia has a fossil record predating 65 Ma ([20], [22]).
32. M. S. Springer, W. J. Murphy, E. Eizirik, S. J. O'Brien, *Proc. Natl. Acad. Sci. U.S.A.* **100**, 1056 (2003).
33. We thank R. Andrews and D. Kent for discussions. Our research is supported by the NSF through Biocomplexity grant OCE-0084032.

Preindustrial to Modern Interdecadal Variability in Coral Reef pH

Carles Pelejero,[1]*† Eva Calvo,[1]*† Malcolm T. McCulloch,[1]† John F. Marshall,[1] Michael K. Gagan,[1] Janice M. Lough,[2] Bradley N. Opdyke[3]

The oceans are becoming more acidic due to absorption of anthropogenic carbon dioxide from the atmosphere. The impact of ocean acidification on marine ecosystems is unclear, but it will likely depend on species adaptability and the rate of change of seawater pH relative to its natural variability. To constrain the natural variability in reef-water pH, we measured boron isotopic compositions in a ~300-year-old massive *Porites* coral from the southwestern Pacific. Large variations in pH are found over ~50-year cycles that covary with the Interdecadal Pacific Oscillation of ocean-atmosphere anomalies, suggesting that natural pH cycles can modulate the impact of ocean acidification on coral reef ecosystems.

Since the beginning of the industrial revolution, the burning of fossil fuels has increased the CO_2 content of the atmosphere from ~280 to more than 370 parts per million per volume (ppmv), a level unprecedented in the last 420,000 years ([1]). To date, a large part of anthropogenic CO_2 emissions has been absorbed by the oceans ([2]), which have become

more acidic, thus reducing their capacity to continue to absorb CO_2. Estimates of global oceanic pH trends to the year 2000 indicate that the oceans have already acidified by 0.1 pH units relative to preindustrial times ([3], [4]). Geochemical models forecast an exponential decrease of nearly 0.8 pH units by 2300 ([4]), a scenario for which there is no obvious
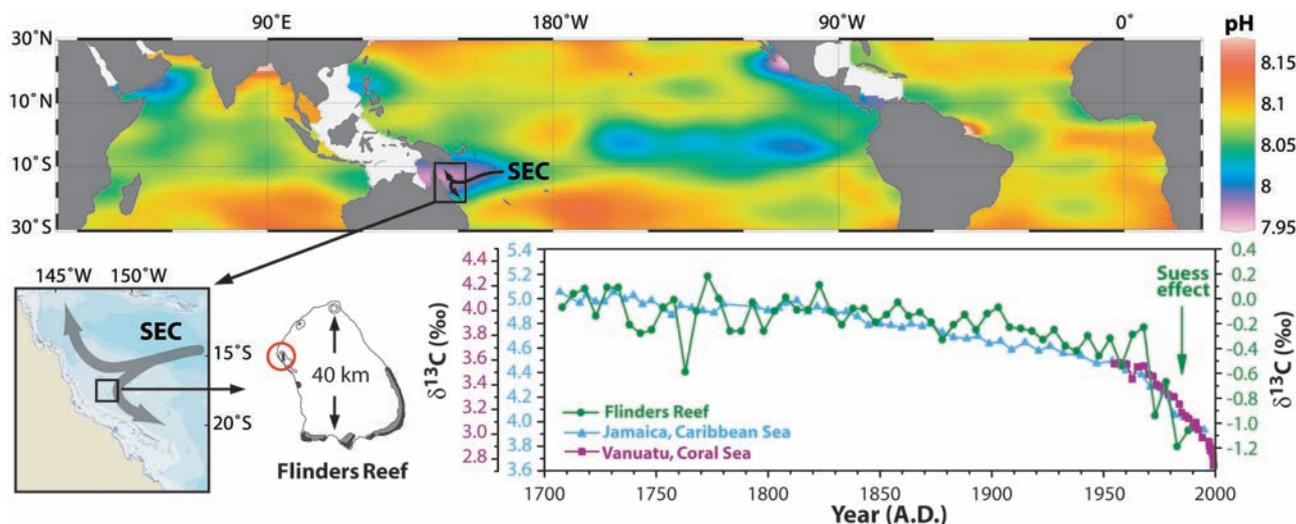
Fig. 1. Distribution of present-day surface-ocean pH, location of the Flinders Reef coral site, and record of coral δ¹³C since 1708 A.D. (**Top**) Map showing present-day mean annual surface pH (*24*). (**Left**) Locality map showing Flinders Reef and approximate path of the SEC and sketch showing the location and dimensions of Flinders Reef. Coral core FL02A was drilled on the North West Reef (17.5°S, 148.3°E; red circle). (**Right**) The δ¹³C data for the Flinders Reef coral and coralline sponges, *Ceratoporella nicholsoni* (Jamaica) (*25*) and *Acanthochaetes wellsi* (Vanuatu) (*26*), show a progressive depletion of ¹³C in surface seawater, which can be ascribed to the Suess effect.

precedent over the last hundreds of millions of years (*5*), with the possible exception of abrupt changes such as those associated with the Paleocene/Eocene Thermal Maximum 55.5 million years ago (*6*). Experimental evidence indicates that such reductions in surface-ocean pH and carbonate saturation state could have major effects on calcifying marine biota (*7*), especially calcareous plankton (*8*) and coral reef communities, where the degree of carbonate supersaturation has been shown to have a major effect on calcification rates (*9–11*).

The actual trend and range of natural variability in oceanic pH remains largely unknown, yet it is crucial to understand the possible consequences of acidification on marine ecosystems. A reliable proxy record is needed to assess long-term trends and variability in seawater pH. Instrumental records of the seawater CO₂ system, such as those collected at the Hawaii Ocean Time Series Station, which only commenced in 1989 (*12*), are short. In this Report, we present a reconstruction of seawater pH spanning the last three centuries, based on the boron isotopic composition (δ¹¹B) (*13*) of a long-lived massive coral (*Porites*) from Flinders Reef in the western Coral Sea (Fig. 1).

The potential of δ¹¹B in biogenic carbonates as a proxy for paleo-pH was first re-

alized during the early 1990s (*14, 15*), and reconstructions of seawater pH using foraminifera have since been reported (*16–19*). Although the feasibility of using δ¹¹B in corals to track changes in pH has been appreciated (*14, 15, 20, 21*), no long-term continuous records of coral δ¹¹B-derived pH have been reported. Culture experiments on *Porites* and *Acropora* have confirmed that corals faithfully record variations in seawater pH (*22, 23*), but there is still some uncertainty about how "vital" effects associated with coral calcification may influence pH proxy records (*22*). The calibration of δ¹¹B ratios with seawater pH for *Porites* grown under controlled conditions is in good agreement with the theoretical curve for the borate species (*22*), the major form in which boron is incorporated into coral skeletons (*14, 15*). In this study, we determined a record of seawater pH from δ¹¹B ratios for a *Porites* coral (*24*) from Flinders Reef in the Coral Sea (Fig. 2A and fig. S1). The full length of the coral core was sampled in 5-year increments, providing a continuous record of seawater pH that commences in 1708 A.D., well before the start of the Industrial Revolution. This record provides a natural baseline against which the long-term effects of ocean acidification on reef-water pH can be assessed.

Figure 1 shows the coral δ¹³C record for the period 1708 to 1988 A.D., derived from the same 5-year sample increments as those analyzed for δ¹¹B (*24*). The most notable feature of the δ¹³C curve is the trend toward lower values commencing from 1800 A.D. Similar trends have been recorded in sclerosponges from Jamaica in the Caribbean Sea and from Vanuatu in the Coral Sea (*25, 26*) (Fig. 1). The secular decrease in coral δ¹³C

can be ascribed to the Suess effect, which is due to uptake by the oceans of atmospheric CO₂ that has been progressively depleted in ¹³C by combustion of fossil fuels.

Although the lowest δ¹¹B value for the entire record corresponds to the 5-year average around 1988 [23.0 per mil (‰), 7.91 pH units; Fig. 2A and table S1], there is no notable trend toward lower δ¹¹B values. The dominant feature of the coral δ¹¹B record is a clear interdecadal oscillation of pH, with δ¹¹B values ranging between 23 and 25‰ (7.9 and 8.2 pH units; Fig. 2A). Spectral analysis of the coral pH record demonstrates a substantial cyclicity of about 50 years (Fig. 2A and fig. S2). Moreover, the variation in pH is synchronous with the Interdecadal Pacific Oscillation (IPO) (*27*), the Pacific-wide equivalent of the Pacific Decadal Oscillation (PDO) (*28*), which is also well represented by a 50- to 70-year cyclicity (*29*) (Fig. 2B and fig. S2). The IPO is well represented by a spatial pattern of sea surface temperature (SST) anomalies over the Pacific Ocean, such that the index is positive when the equatorial Pacific is warm and the southwest Pacific and central North Pacific are cold. This pattern of interdecadal climate variability shares similarities with the El Niño-Southern Oscillation (ENSO), with periods of positive and negative IPO values displaying climatic patterns similar to El Niño and La Niña, respectively (*30, 31*).

The covariation of the Flinders paleo-pH record and the IPO provides insight into possible mechanisms driving long-term interdecadal variation in seawater pH at the study site. One mechanism for lowering pH could be vertical mixing and upwelling of subsurface (hence more acidic) waters during periods

¹Research School of Earth Sciences, The Australian National University, Canberra, ACT 0200, Australia. ²Australian Institute of Marine Science, PMB #3, Townsville Mail Centre, QLD 4810, Australia. ³Department of Earth and Marine Sciences, The Australian National University, Canberra, ACT 0200, Australia.

*Present address: Institut de Ciències del Mar, CMIMA-CJIC, 08003 Barcelona, Catalonia, Spain.
†To whom correspondence should be addressed. E-mail: pelejero@cmima.csic.es (C.P.); ecalvo@cmima.csic.es (E.C.); Malcolm.McCulloch@anu.edu.au (M.T.M.)

2205

of positive IPO. However, upwelling would produce SSTs substantially cooler than average, which is inconsistent with the coral Sr/Ca record given that there is no correlation between Sr/Ca and pH (32). Also, upwelled low pH water would bring cooler and saltier Subtropical Lower Waters to the surface, as observed during upwelling intrusions into the Great Barrier Reef (33). However, paleosalinity estimates from coupled analysis of coral $\delta^{18}O$ and Sr/Ca in the Flinders Reef coral (24) indicate that there is no correlation between low pH and high salinity (32).

Given the present-day differences observed in surface-ocean pH throughout the tropical Pacific (~0.2 units; Fig. 1), interdecadal changes in surface currents and the redistribution of water masses could be another factor affecting surface-ocean pH. The stronger and/or more frequent La Niña events that develop during times of negative IPO (30) would enhance the strength of the South Equatorial Current (SEC) (34) and bring higher pH surface waters into the Flinders Reef area, in agreement with the coral $\delta^{11}B$ record (Fig. 2). However, this could not account for the full range of pH variability

(~0.3 units) inferred from the Flinders Reef coral.

The most likely explanation for the variability in pH at Flinders Reef is that coral reef calcification combined with limited flushing of reef water exerts an important local control over the extent of the buildup of partial pressure of CO_2 (P_{CO_2}) within the reef. This is consistent with observations at other reefs, such as those in the Indo-Pacific region (35), where the residence time of lagoon water influences the carbon budget of reef water. Flinders Reef is also likely to be influenced by these processes because it is one of the largest discrete reef systems in the Coral Sea, about 40 km north to south, with a continuous barrier of about 15 km along the eastern side (Fig. 1). The platform reef is directly flushed by the SEC (Fig. 1), whose strength is proportional to Pacific trade-wind velocity, which ultimately controls the exchange of Flinders Reef water with the open ocean. During periods of positive IPO (similar to El Niño) when the Pacific tradewinds and SEC are relatively weak (34), renewal of the Flinders Reef water would also be slower and the consequent buildup of CO_2 through calcification would lower the ambient seawater pH. This is the same phase in which the IPO and Flinders Reef pH are correlated, with positive IPO corresponding to low pH and negative IPO corresponding to high pH (Fig. 2). Moreover, changes in western Pacific sea level with the ENSO phase [up to ~30 cm in areas of the South Equatorial Pacific (34)] would also affect the rate of exchange of lagoonal water at Flinders Reef. During positive IPO phases (similar to El Niño), lower sea levels would further reduce the renewal of reef waters, thus enhancing the buildup of CO_2 and lowering pH. In contrast, more efficient flushing of reef water during the negative IPO phase (similar to La Niña) would explain the higher pH values (Fig. 2).

High-resolution analysis of $\delta^{11}B$ in the Flinders Reef coral provides a seasonal record of reef-water pH that lends support to this mechanism (Fig. 2C). The seasonal pH record, spanning April 1987 to April 1988, shows a tendency to covary with wind speed recorded nearby at Willis Island (16.3°S, 150.0°E), where strong winds occur at times of high seawater pH and weak winds occur at times of low seawater pH at Flinders Reef (Fig. 2). The seasonal rise in reef-water pH (March/April) also coincides with the seasonal intensification of the SEC (36). Conversely, pH displays minimum values from October to March, when the SEC is weaker (36), allowing for a buildup of reef-water CO_2. This mechanism explains the lower seawater pH values for Flinders Reef relative to open ocean waters; it is only at times of efficient lagoonal flushing (e.g., ~1960 A.D.) that reef-water pH reaches values typical of the open ocean (pH = ~8.1 to 8.2).
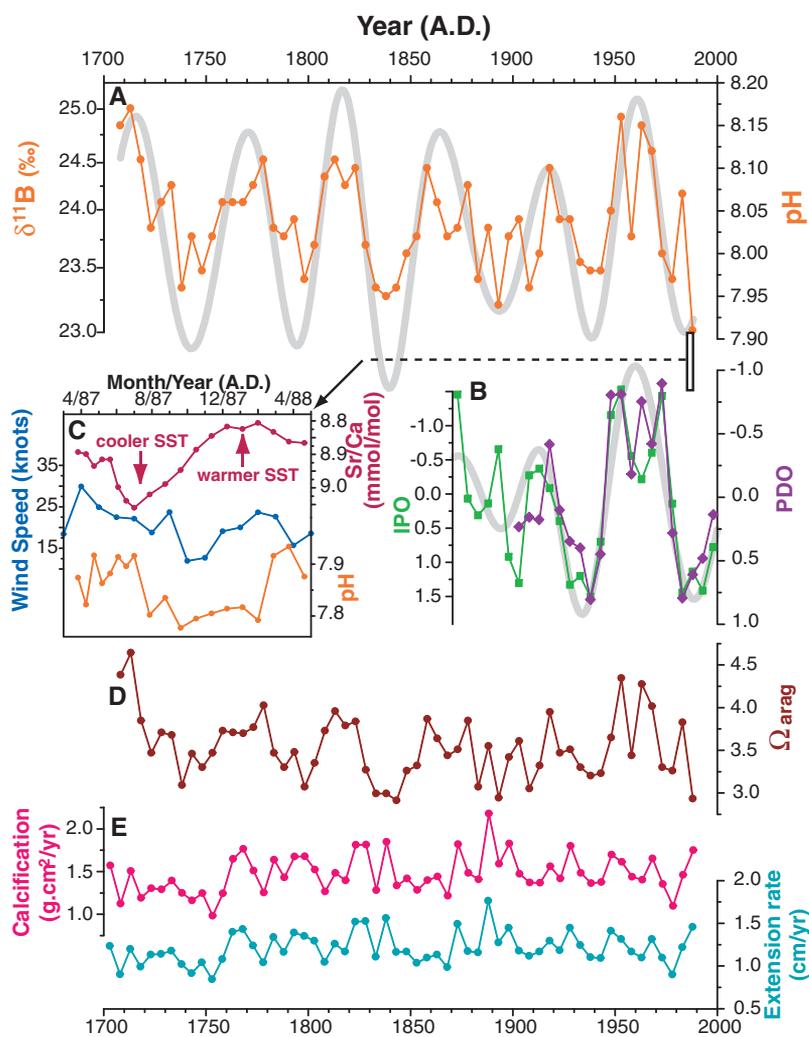

Fig. 2. Record of Flinders Reef coral $\delta^{11}B$, reconstructed oceanic pH, aragonite saturation state, PDO and IPO indices, and coral calcification parameters. (**A**) Flinders Reef coral $\delta^{11}B$ as a proxy for surface-ocean pH (24); $\delta^{11}B$ measurements for all 5-year intervals are available in table S1. (**B**) Indices of the PDO (28, 39) and the IPO (27) averaged over the same 5-year intervals as the coral pH data. Gray curves in panels (A) and (B) are the outputs of Gaussian filtering of coral pH and IPO values, respectively, at a frequency of 0.02 ± 0.01 year⁻¹, which represent the 1/50-year component of the pH variation (fig. S2). (**C**) Comparison of high-resolution coral Sr/Ca (plotted to identify the seasonal cycle of SST) (32), $\delta^{11}B$-derived pH, and wind speed recorded at the Willis Island meteorological station (data from the Australian Bureau of Meteorology) (40). Note the covariation of wind speed and seawater pH; strong winds generally occur at times of high pH, and weak winds generally occur at times of low pH. All high-resolution $\delta^{11}B$ measurements are available in table S2. (**D**) Aragonite saturation state, $\Omega_{arag} = [Ca^{2+}][CO_3^{2-}]/K'_{sp}$, where K'_{sp} is the stoichiometric solubility product of aragonite, calculated from our reconstructed pH assuming constant alkalinity (24). (**E**) Coral extension and calcification rates obtained from coral density measured by gamma ray densitometry (38).

Regardless of the mechanism controlling reef-water pH, our results suggest that corals at Flinders Reef have experienced a relatively wide range in pH (~0.3 pH units) over the past ~300 years. As a result, these corals have also experienced equivalent changes in the aragonite saturation state (Ω_{arag}), one of the main physicochemical controllers of coral calcification. Changes in Ω_{arag} have been derived from the Flinders pH record (Fig. 2D), with Ω_{arag} varying from ~3 to 4.5, assuming constant alkalinity (10, 24). This encompasses the lower and upper limits of Ω_{arag} within which corals can survive (37). Despite such marked changes, skeletal extension and calcification rates for the Flinders Reef coral (Fig. 2E) fall within the normal range for *Porites* (38) and are not correlated with Ω_{arag} or pH. Therefore, the *Porites* coral at Flinders Reef seems well adapted to relatively large fluctuations in seawater pH and Ω_{arag}.

The interdecadal cycle in seawater pH observed at Flinders Reef has relevance for predicting its response to future ocean acidification, given that it will either enhance or moderate the local effects of the projected long-term decrease in pH (3, 4). For example, the next rise in the ~50-year cycle of reef-water pH should counteract the lowering of pH values at Flinders Reef until ~2035 A.D. Conversely, the subsequent fall in the reef-water pH cycle will lead to an abrupt shift toward low pH reef water. The extent to which corals and other calcifying reef organisms can adapt to such rapid decreases in pH is largely unknown.

Our findings suggest that the effects of progressive acidification of the oceans are likely to differ between coral reefs because reef-water P_{CO_2} and consequent changes in seawater pH will rarely be in equilibrium with the atmosphere. Although the relatively large variations in seawater pH at Flinders Reef suggest that coral reefs may be resilient to the shorter term effects of ocean acidification, in the coming decades many reefs are likely to experience reduced pH that is unprecedented relative to "natural" levels. Additional paleo-pH records are required from a range of coral reef ecosystems to improve our understanding of the physical and biological controls on reef-water pH, and the long-term impacts of future ocean acidification.

References and Notes

1. J. R. Petit *et al.*, *Nature* **399**, 429 (1999).
2. C. L. Sabine *et al.*, *Science* **305**, 367 (2004).
3. D. A. Wolf-Gladrow, U. Riebesell, S. Burkhardt, J. Bijma, *Tellus* **51B**, 461 (1999).
4. K. Caldeira, M. E. Wickett, *Nature* **425**, 365 (2003).
5. A. Ridgwell, R. E. Zeebe, *Earth Planet. Sci. Lett.* **234**, 299 (2005).
6. J. C. Zachos *et al.*, *Science* **308**, 1611 (2005).
7. R. A. Feely *et al.*, *Science* **305**, 362 (2004).
8. U. Riebesell *et al.*, *Nature* **407**, 364 (2000).
9. J. P. Gattuso, D. Allemand, M. Frankignoulle, *Am. Zool.* **39**, 160 (1999).
10. J. A. Kleypas *et al.*, *Science* **284**, 118 (1999).
11. F. Marubini, M. J. Atkinson, *Mar. Ecol. Prog. Ser.* **188**, 117 (1999).
12. J. Dore, R. Lukas, D. Sadler, D. M. Karl, *Nature* **424**, 754 (2003).
13. Data are reported with the delta notation relative to the National Bureau of Standards (NBS) 951 boric acid standard defined as $\delta^{11}B$ (‰) = (Rs/Rstd − 1) × 1000, where Rs = $^{11}B/^{10}B$ of the sample and Rstd = $^{11}B/^{10}B$ of NBS 951. External precision of $\delta^{11}B$ values are estimated at ±0.2‰ ($2\sigma_{mean}$ level) (24).
14. A. Vengosh, Y. Kolodny, A. Starinsky, A. R. Chivas, M. T. McCulloch, *Geochim. Cosmochim. Acta* **55**, 2901 (1991).
15. N. G. Hemming, G. N. Hanson, *Geochim. Cosmochim. Acta* **56**, 537 (1992).
16. A. J. Spivack, C.-F. You, J. Smith, *Nature* **363**, 149 (1993).
17. A. Sanyal, N. G. Hemming, G. N. Hanson, W. S. Broecker, *Nature* **373**, 234 (1995).
18. P. N. Pearson, M. R. Palmer, *Science* **284**, 1824 (1999).
19. M. R. Palmer, P. N. Pearson, *Science* **300**, 480 (2003).
20. J. Gaillardet, C. Jean Allègre, *Earth Planet. Sci. Lett.* **136**, 665 (1995).
21. N. G. Hemming, T. P. Guilderson, R. G. Fairbanks, *Global Biogeochem. Cycles* **12**, 581 (1998).
22. B. Hönisch *et al.*, *Geochim. Cosmochim. Acta* **68**, 3675 (2004).
23. S. Reynaud, N. G. Hemming, A. Juillet-Leclerc, J. P. Gattuso, *Coral Reefs* **23**, 539 (2004).
24. Materials and methods are available as supporting material on *Science* Online.
25. F. Böhm *et al.*, *Geochem. Geophys. Geosyst.* **3**, 10.1029/2001GC000264 (2002).
26. S. J. Fallon, T. P. Guilderson, K. Caldeira, *Geophys. Res. Lett.* **30**, 10.1029/2003GL018049 (2003).
27. S. Power, T. Casey, C. K. Folland, A. Colman, V. Mehta, *Clim. Dyn.* **15**, 319 (1999).
28. N. J. Mantua, S. R. Hare, *J. Oceanogr.* **58**, 35 (2002).
29. S. Minobe, *Geophys. Res. Lett.* **24**, 683 (1997).
30. M. J. Salinger, J. Renwick, A. B. Mullan, *Int. J. Climatol.* **21**, 1705 (2001).
31. A. Gershunov, T. P. Barnett, *Bull. Am. Meteorol. Soc.* **79**, 2715 (1998).
32. E. Calvo *et al.*, in preparation.
33. J. C. Andrews, M. J. Furnas, *Cont. Shelf Res.* **6**, 491 (1986).
34. M. A. Cane, *Science* **222**, 1189 (1983).
35. A. Suzuki, H. Kawahata, *Tellus B* **55**, 428 (2003).
36. B. A. Taft, W. S. Kessler, *J. Geophys. Res.* **96**, 12599 (1991).
37. J. A. Kleypas, J. W. McManus, L. A. B. Menez, *Am. Zool.* **39**, 146 (1999).
38. J. M. Lough, D. J. Barnes, *J. Exp. Mar. Biol. Ecol.* **211**, 29 (1997).
39. PDO index data (available at ftp://ftp.atmos.washington.edu/mantua/pnw_impacts/INDICES/PDO.latest).
40. Australian Government, Bureau of Meteorology (www.bom.gov.au).
41. We thank L. Kinsley for assistance with Triton mass spectrometry at Research School of Earth Sciences, S. Power and the UK Met. Office for providing the IPO data and W. Müller, E. Hendy, G. Foster, C. Coath, B. Windel, B. Hönisch, A. Suzuki, R. Key, T. McConnaughey, M. Church, J. Dore, and L. Pena for stimulating discussions and help throughout this research. Australian Postdoctoral Fellowships awarded to C.P. and E.C. (Australian Research Council grants DP0342702 and DP0450682) are gratefully acknowledged. C.P. and E.C. also acknowledge funding from the Spanish Ministry of Education and Science during the early stages of this work. The coral drilling by Peter Isdale and Bruce Parker, Australian Institute of Marine Science, was funded by an Australian National Greenhouse Advisory Committee grant to J. Chappell. The data will be made available on the NOAA Paleoclimatology Web site (www.ngdc.noaa.gov/paleo/data.html).

Phylogenetic MCMC Algorithms Are Misleading on Mixtures of Trees

Elchanan Mossel[1] and Eric Vigoda[2]

Markov chain Monte Carlo (MCMC) algorithms play a critical role in the Bayesian approach to phylogenetic inference. We present a theoretical analysis of the rate of convergence of many of the widely used Markov chains. For *N* characters generated from a uniform mixture of two trees, we prove that the Markov chains take an exponentially long (in *N*) number of iterations to converge to the posterior distribution. Nevertheless, the likelihood plots for sample runs of the Markov chains deceivingly suggest that the chains converge rapidly to a unique tree. Our results rely on novel mathematical understanding of the log-likelihood function on the space of phylogenetic trees. The practical implications of our work are that Bayesian MCMC methods can be misleading when the data are generated from a mixture of trees. Thus, in cases of data containing potentially conflicting phylogenetic signals, phylogenetic reconstruction should be performed separately on each signal.

Bayesian inference is one of the most popular methods in phylogeny reconstruction (1). Many widely used software packages, such as MrBayes (2), BAMBE (3), and PAML (4), rely on Markov chain Monte Carlo (MCMC) methods. These algorithms are often known as BMCMC. Part of the appeal of BMCMC is that they are supposed to be more robust and faster than standard maximum likelihood approaches. Our results show that these appealing features are overly optimistic in some settings.

The basis of the MCMC algorithms is a Markov chain whose stationary distribution is the desired posterior distribution. Reliable phylogenetic estimates depend on the Markov chain converging to the posterior distribution